Exact Method of Designing Airfoils With Given Velocity Distribution in Incompressible Flow

T. Strand*
Air Vehicle Corp., San Diego, Calif.

The inverse problem of airfoil theory, i.e., from a given surface velocity distribution determine the airfoil shape, is solved by conformal mapping procedures. The method is based upon prior work by Arlinger, which in turn is an extension of Lighthill's basic development. It involves the use of least squares and Lagrangian multipliers to modify the prescribed velocity distribution along a portion of the lower surface of the airfoil, thus ensuring that the modifications required for profile closure are minimized. The method developed should be of particular importance for calculating the shapes of new types of airfoils with high design lift coefficients, i.e., under conditions when conventional linearized theory breaks down. The method is exact in the sense of potential flow theory. Sample calculations are presented for a prescribed velocity distribution having an upper-surface constant-velocity region, followed by a Stratford-type zero-skin-friction portion, designed for Reynolds number = 3.10^6 and turbulent flow on both upper and lower surfaces.

Nomenclature

b = constant
C_k = constants
C_L = lift coefficient
C_m = moment coefficient
c = chord
F = complex potential function ($= \varphi + i\psi$)
G = portion of the circulation integral
i = $(-1)^{1/2}$
Γ = circulation strength
H = least squares function
M = minimizing function
R = radius of circle
r = radius of curvature at the leading edge
s = distance along airfoil surface, measured counterclockwise from trailing edge
t = maximum thickness of airfoil
w = velocity magnitude
z = complex coordinate in airfoil plane ($= x + iy$)
α = angle-of-attack
ζ = complex coordinate in circle plane ($= \xi + i\eta$)
θ = polar coordinate in circle plane
ν = angle of the velocity vector anywhere in the circle plane
τ = angle of the velocity vector anywhere in the airfoil plane
ϵ = small polar angle in circle plane ($\epsilon << 1$)

Subscripts

a = airfoil plane
c = circle plane, or chord
d = design
0 = original, or zero-lift
∞ = infinity

I. Introduction

A series of new airfoils designed for maximum lift is presented in Ref. 1. Lift/drag ratios as high as 350 are shown at design lift coefficients in excess of 2.5, assuming laminar flow, except for a zero-skin friction portion along the upper surface. The airfoils exhibit maximum velocities in excess of twice the freestream velocity, and were designed by second-order linearized flow theory. With such high surface velocities the region of validity of linearized theory might well be exceeded, precluding good agreement between theory and experiment. Reference 1 also includes one graph showing that a discrepancy exists between the prescribed velocity distribution and that calculated by an exact direct method (the Douglas Neumann method) for the contour obtained by the second-order inverse program. No really satisfactory exact inverse method yet exists for computing profile shapes from a specified velocity distribution.

Previous authors have tried to develop exact methods for this problem. For instance, the method given in Ref. 2 is exact in the sense of potential flow. However, here the velocity distribution must be selected as a function of the angle in the circle plane into which the profile is mapped, rather than as a function of the distance along the surface. This method is therefore of very limited usefulness as a design tool.

Arlinger[3] recently extended the ideas of Ref. 2, to be able to specify the velocities as a function of distance along the surface. The method involves the subsequent modification of the input velocity distribution along the lower surface, so as to obtain a closed curve for the resulting airfoil. To assure closure at the trailing edge, three integral equations, first given by Lighthill, must be satisfied. Arlinger employs a three-term sine series with three unknown coefficients for this purpose. Unless the input lower-surface velocity distribution is quite close to the final acceptable distribution, one or more of the three coefficients become large, completely altering the input velocity distribution along the lower surface between the stagnation point and the trailing edge.

In the next section the Lighthill and Arlinger methods have been further developed by adding a method for minimizing the excursions of the modified velocity distribution from the given distribution along the lower surface, thereby obtaining a consistently acceptable distribution that is as close as possible, in a least squares sense, to that given. Initially the development in the next section is almost identical to that of Arlinger.

II. Theory

A. Calculation of $w_a(\theta)$

The coordinate systems and symbols used are shown in Fig. 1. The airfoil in the z-plane ($z = x + iy$) corresponds

Received December 18, 1972; revision received April 25, 1973. The research was performed under U.S. Navy Contract N00600-71-C-0709.The author is indebted to T. T. Yeh for several valuable suggestions and for programming the method on the digital computer.

Index categories: Subsonic and Transonic Flow; Hydrodynamics; Aircraft Aerodynamics (Including Component Aerodynamics).

*Corporation President. Associate Fellow AIAA.

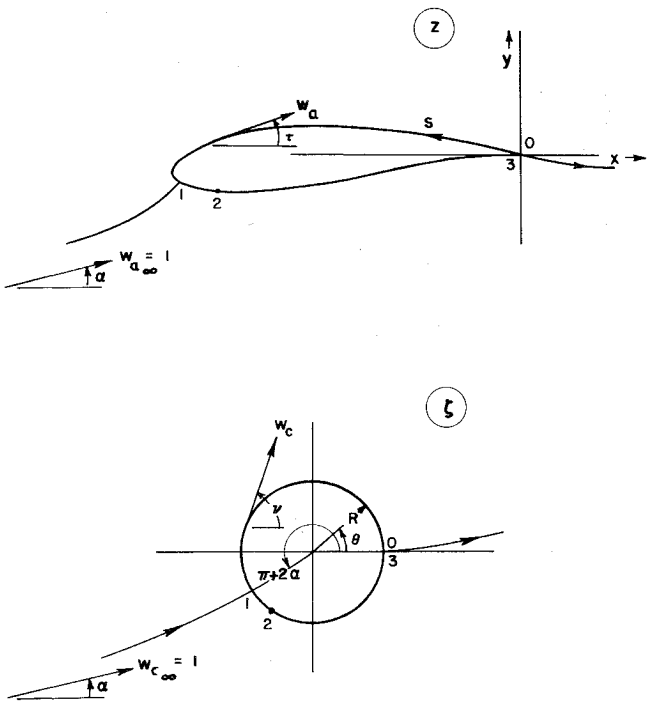

Fig. 1. Conformal mapping planes and coordinate systems.

conformally to a circle of radius R in the ζ-plane ($\zeta = \xi + i\eta$). The trailing edge of the airfoil is transformed into the point $(R,0)$ in the ζ-plane. The flowfield in the ζ-plane is known. The velocities at infinity in both mapping planes are uniform with magnitude unity and inclination α to the positive x- and ξ-axes.

The magnitude $w_a(s)$ of the velocity along the airfoil surface is prescribed. The circulation Γ may then be calculated, i.e.,

$$\Gamma = \int_0^{s_1} w_a ds - \int_{s_1}^{s_3} w_a ds \tag{1}$$

The distance s along the surface is measured from the trailing edge in a counterclockwise direction. The distances s_1 and s_3 refer to the distance from the trailing edge to the leading-edge stagnation point and to the trailing edge, respectively.

Let F denote the complex potential function. The relation between the conjugate velocities at corresponding points anywhere in the flow fields of the two planes may be expressed as follows:

$$w_a e^{-i\tau} = \frac{dF}{dz} = \frac{dF}{d\zeta}\frac{d\zeta}{dz} = w_c e^{-i\nu}\frac{d\zeta}{dz} \tag{2}$$

Taking absolute values, Eq. (2) yields for points on the airfoil and circle

$$w_a ds = w_c R d\theta \tag{3}$$

where R is the radius of the circle.

To determine expressions for w_c, R, and α, we superimpose in the ζ-plane a uniform stream, a doublet, and a vortex in the usual manner, i.e.,

$$F = e^{-i\alpha}\zeta + R^2 e^{i\alpha}/\zeta + (i\Gamma/2\pi)\ln\zeta \tag{4}$$

Requiring the rear stagnation point to be at $(R,0)$, we find a second expression for the circulation

$$\Gamma = 4\pi R \sin\alpha \tag{5}$$

Substitution of this Γ into Eq. (4) yields the conjugate velocity on the circle, as follows:

$$w_c e^{-i\nu} = \frac{dF}{d\zeta} = 2ie^{-i\theta}[\sin(\theta - \alpha) + \sin\alpha] \tag{6}$$

Hence,

$$\left.\begin{aligned} w_c &= 2[\sin(\theta - \alpha) + \sin\alpha] \\ \nu &= \theta - \pi/2 \end{aligned}\right\} 0 \le \theta \le \pi + 2\alpha \tag{7}$$

and

$$\left.\begin{aligned} w_c &= -2[\sin(\theta - \alpha) + \sin\alpha] \\ \nu &= \theta + \pi/2 \end{aligned}\right\} \pi + 2\alpha \le \theta \le 2\pi \tag{8}$$

It is noted that the two stagnation points are located at $\theta = 0$ and $\pi + 2\alpha$.

Next, define G_{01} as the following known integral.

$$G_{01} = \int_0^{s_1} w_a ds \tag{9}$$

Integrating Eq. (3) and employing Eq. (7), a second expression for G_{01} is determined

$$G_{01} = \int_0^{\pi+2\alpha} w_c R d\theta = 2R[2\cos\alpha + (\pi + 2\alpha)\sin\alpha] \tag{10}$$

Combining Eqs. (5) and (10), we obtain an implicit solution for α, i.e., for $\Gamma \neq 0$,

$$\tan\alpha = \frac{1}{\pi[(G_{01}/\Gamma) - (1/2)] - \alpha} \tag{11}$$

The radius of the circle may now, for instance, be found from Eq. (5). Thus, w_c, R, and the design angle α are now known and will remain fixed throughout the subsequent development.

Next let us obtain the correspondence between the surface distances s and $R\theta$ in the two mapping planes. Integration of Eq. (3), using Eqs. (7) and (8), yields the following relations, expressed in a form convenient for numerical calculation

$$\int_0^s w_a ds = 2R[\cos\alpha - \cos(\theta - \alpha) + \theta\sin\alpha] \quad \text{for } 0 \le s \le s_1,\ 0 \le \theta \le \pi + 2\alpha, \tag{12}$$

$$\int_{s_1}^s w_a ds = 2R[\cos\alpha + \cos(\theta - \alpha) - (\theta - \pi - 2\alpha)\sin\alpha] \quad \text{for } s_1 \le s \le s_3,\ \pi + 2\alpha \le \theta \le 2\pi \tag{13}$$

The left hand side is known. The right hand side is determined numerically with θ being the unknown. It should perhaps be mentioned that the sum of the above two integrals equals $8R$ ($\cos\alpha + \alpha\sin\alpha$) when the integration is performed around the circle. The sum is therefore not in the limit equal to the circulation integral Γ.

From Eqs. (12) and (13), the correspondence between the surface distances s and $R\theta$ is known. Specifically the given distance s_2 from the origin to a point on the lower

surface of the airfoil yields a certain value for θ_2. We further note that w_a is now also known as a function of θ.

B. Modification of $w_a(\theta)$

The set of w_a values as a function of θ must be modified in a certain correction interval if the airfoil shall close at the trailing edge. The set of w_a, determined above, will here be modified in the interval

$$s_2 \leq s \leq s_3, \quad \theta_2 \leq \theta \leq 2\pi$$

The boundary conditions state that $w_a = w_c = 1$ and $\tau = \nu = \alpha$ at infinity. Hence, using Eq. (2),

$$\lim_{\zeta \to \infty} dz/d\zeta = 1 \tag{14}$$

which means that z may be expanded in the following series.

$$z = \zeta + a_0 + \frac{a_1}{\zeta} + \frac{a_2}{\zeta^2} + \ldots \tag{15}$$

Differentiating, we find

$$\frac{dz}{d\zeta} = 1 - \frac{a_1}{\zeta^2} - \frac{2a_2}{\zeta^3} - \ldots = \frac{dF}{d\zeta} \Big/ \frac{dF}{dz} \tag{16}$$

Solving Eq. (16) for dF/dz, and making use of Eq. (4), we have

$$\frac{dF}{dz} = \frac{dF}{d\zeta}\left[1 + \frac{a_1}{\zeta^2} + \frac{2a_2}{\zeta^3} + \ldots\right]$$

$$= e^{-i\alpha}\left[1 + \frac{i\Gamma e^{i\alpha}}{2\pi\zeta} - \frac{R^2 e^{i2\alpha}}{\zeta^2}\right]\left[1 + \frac{a_1}{\zeta^2} + \frac{2a_2}{\zeta^3} + \ldots\right]$$

$$= e^{-i\alpha}\left[1 + \frac{i\Gamma e^{i\alpha}}{2\pi\zeta} + 0\left(\frac{1}{\zeta^2}\right)\right] \tag{17}$$

from which, by Eq. (5)

$$w_a e^{-i(\tau-\alpha)} = 1 + \frac{R(-2\sin^2\alpha + i\sin 2\alpha)}{\zeta} + 0\left(\frac{1}{\zeta^2}\right) \tag{18}$$

It is necessary to split dF/dz into two separate functions since only w_a is prescribed. We therefore expand the above expression into a product of exponential functions; i.e., we let

$$w_a e^{-i(\tau-\alpha)} = \exp\left(\frac{b_1}{\zeta} + \frac{b_2}{\zeta^2} + \frac{b_3}{\zeta^3} + \ldots\right)$$

$$= \left(1 + \frac{b_1}{\zeta} + \frac{b_1}{2\zeta^2} + \ldots\right)\left(1 + \frac{b_2}{\zeta^2} + \frac{b_2}{2\zeta^4} + \ldots\right) \times \left(1 + \frac{b_3}{\zeta^3} + \ldots\right.$$

$$= 1 + \frac{b_1}{\zeta} + 0\left(\frac{1}{\zeta^2}\right) \tag{19}$$

Thus,

$$\ln w_a - i(\tau - \alpha) = \frac{b_1}{\zeta} + \frac{b_2}{\zeta^2} + \ldots \tag{20}$$

On the circle, ζ equals $Re^{i\theta}$, and Eq. (20) becomes

$$\ln w_a - i(\tau - \alpha) = (b_1/R)(\cos\theta - i\sin\theta) + (b_2/R^2)(\cos 2\theta - i\sin 2\theta) + \ldots \tag{21}$$

Hence, defining $b_1 = b_{11} + ib_{12}$, we obtain the following Fourier series for $\ln w_a$

$$\ln w_a = (b_{11}/R)\cos\theta + \ldots + (b_{12}/R)\sin\theta + \ldots \tag{22}$$

where the first two terms only in the series are shown. The three first Fourier coefficients are then given by

$$0 = \frac{1}{\pi}\int_0^{2\pi} \ln w_a d\theta$$

$$\frac{b_{11}}{R} = \frac{1}{\pi}\int_0^{2\pi} \ln w_a \cos\theta d\theta$$

$$\frac{b_{12}}{R} = \frac{1}{\pi}\int_0^{2\pi} \ln w_a \sin\theta d\theta \tag{23}$$

Comparison of Eqs. (18) and (19) yields by inspection $b_{11} = -2R\sin^2\alpha$ and $b_{12} = R\sin 2\alpha$. Substitution into Eq. (23) finally results in the following three constraint equations for w_a

$$\int_0^{2\pi} \ln w_a d\theta = 0$$

$$\int_0^{2\pi} \ln w_a \cos\theta d\theta = -2\pi\sin^2\alpha$$

$$\int_0^{2\pi} \ln w_a \sin\theta d\theta = \pi\sin 2\alpha \tag{24}$$

The above integral relations were derived previously for $\alpha = 0$ in Ref. 2. The first integral is a consequence of choosing the velocity magnitude equal to unity at infinity. The latter two integrals ensure that the airfoil is closed at the trailing edge.

By Eq. (21), $\tau - \alpha$ may also be expressed in a Fourier series. It is then easily shown that the constraint equations involving τ, which correspond to Eqs. (24) for $\ln w_a$, are:

$$\int_0^{2\pi} \tau d\theta = 2\pi\alpha$$

$$\int_0^{2\pi} \tau \cos\theta d\theta = -\pi\sin 2\alpha$$

$$\int_0^{2\pi} \tau \sin\theta d\theta = -2\pi\sin^2\alpha \tag{25}$$

Equations (25) are not useful in the present development except, maybe, for serving as a check on the accuracy of the set of $\tau(\theta)$ obtained below.

Equations (24) are formally identical to those given in Ref. 3, when the integrations involving w_c are performed. These relations state that w_a must be modified to become acceptable. In Ref. 3 this modification is done by expanding the given w_a in a three-term trigonometric series in the chosen correction interval (the entire lower surface). The three constant coefficients are then determined by substitution into the three constraint equations. It was found that this method is unsuitable, because the three

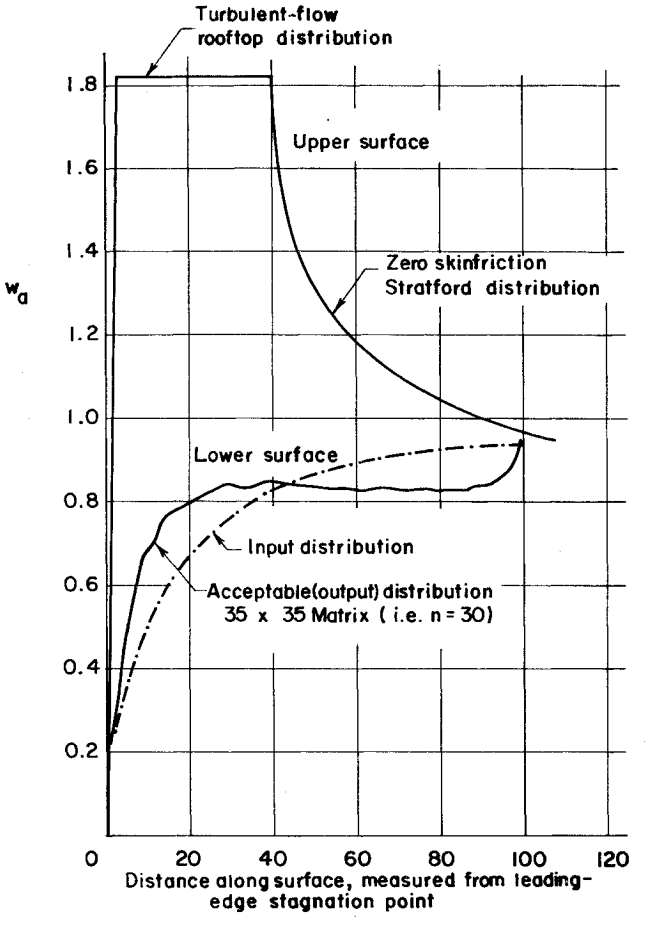

Fig. 2. Velocity distribution for a sample case, Γ = 68. Stratford distribution calculated for $Re = 3.10^6$.

constants tend in general to become very large, causing large undesirable waviness in the modified velocity distribution along the lower surface. With the modified velocity distribution being far from the desired input distribution, the resulting airfoil shapes are quite unsatisfactory. However, the method will yield satisfactory results whenever the input distribution on the lower surface happens to be close to the accepted distribution, which is the case for the airfoils illustrated in Ref. 3.

We now depart from the development of Ref. 3, and use a least squares method to ensure that the modified velocity distribution remains as close as possible to that originally prescribed. Note that the initial point of the correction interval on the lower surface will not be the leading-edge stagnation point, but will be prescribed, i.e. $s_2 > s_1$.

Let us then modify w_a through a system of $n(n \geq 10$, say) linearly independent functions $f_k(\theta)$, where $k = 1,2,3,\ldots,n$, in the interval between $\theta = \theta_2$ and 2π, by defining

$$w_a = w_{ao} e^{\sum_{k=1}^{n} C_k f_k(\theta)} \tag{26}$$

Here w_{a0} denotes the prescribed velocity distribution, and the C_k's are constants to be determined. It is now desired to minimize the excursions of $w_a(\theta)$ from the given $w_{a0}(\theta)$. A new function $H(C_k)$ is therefore defined as follows:

$$H(C_k) = \int_{\theta_2}^{2\pi} \left[\ln \frac{w_a}{w_{ao}} \right]^2 d\theta = \int_{\theta_2}^{2\pi} \left[\sum_{k=1}^{n} C_k f_k(\theta) \right]^2 d\theta \tag{27}$$

where Eq. (26) has been used. The above function is a measure of how well the modified velocity distribution matches the prescribed distribution in the correction interval.

To assure a smooth transition at θ_2, and to tie down the new function at 2π, we shall require that

$$\left.\frac{dw_{ao}}{d\theta}\right|_{\theta_2,2\pi} = \left.\frac{dw_a}{d\theta}\right|_{\theta_2,2\pi} = \left[\frac{dw_{ao}}{d\theta} + w_{ao} \sum_{k=1}^{n} C_k f_k' \right]_{\theta_2,2\pi} \tag{28}$$

where the prime superscript indicates differentiation with respect to θ. Equation (28) then becomes $\Sigma C_k f_k' = 0$ at θ_2 and at 2π.

Introducing Lagrangian multipliers λ_1, λ_2, λ_3, λ_4 and λ_5, and defining another function M, we let

$$\begin{aligned} M(C_k,\lambda_1,\lambda_2,\lambda_3,\lambda_4,\lambda_5) &= H(C_k) + \lambda_1 \int_0^{2\pi} \ln w_a d\theta \\ &+ \lambda_2 [2\pi \sin^2\alpha + \int_0^{2\pi} \ln w_a \cos\theta d\theta] \\ &+ \lambda_3 [-\pi \sin 2\alpha + \int_0^{2\pi} \ln w_a \sin\theta d\theta] \\ &+ \lambda_4 \sum_{k=1}^{n} C_k f_k' \Big|_{\theta_2} + \lambda_5 \sum_{k=1}^{n} C_k f_k' \Big|_{2\pi} \\ = \int_{\theta_2}^{2\pi} [\sum_{k=1}^{n} C_k f_k(\theta)]^2 d\theta &+ \lambda_1 [\int_0^{2\pi} \ln w_{ao} d\theta + \int_{\theta_2}^{2\pi} \sum_{k=1}^{n} C_k f_k(\theta) d\theta] \\ &+ \lambda_2 [2\pi \sin^2\alpha + \int_0^{2\pi} \ln w_{ao} \cos\theta d\theta + \int_{\theta_2}^{2\pi} \sum_{k=1}^{n} C_k f_k(\theta) \cos\theta d\theta] \\ &+ \lambda_3 [-\pi \sin 2\alpha + \int_0^{2\pi} \ln w_{ao} \sin\theta d\theta + \int_{\theta_2}^{2\pi} \sum_{k=1}^{n} C_k f_k(\theta) \sin\theta d\theta] \\ &+ \lambda_4 \sum_{k=1}^{n} C_k f_k' \Big|_{\theta_2} + \lambda_5 \sum_{k=1}^{n} C_k f_k' \Big|_{2\pi} \end{aligned} \tag{29}$$

The extrema of M is obtained when the function fulfills the n + 5 separate equations

$$\frac{\partial M}{\partial C_k} = \frac{\partial M}{\partial \lambda_1} = \frac{\partial M}{\partial \lambda_2} = \frac{\partial M}{\partial \lambda_3} = \frac{\partial M}{\partial \lambda_4} = \frac{\partial M}{\partial \lambda_5} = 0 \qquad k = 1,2,3,.,n \tag{30}$$

The above expression forms a determined system of linear algebraic equations for the determination of $C_1, C_2, \ldots, C_n$ and $\lambda_1, \lambda_2, \ldots, \lambda_5$.

Any set of orthogonal functions might be used for $f_k(\theta)$, as long as $f_k(\theta_2)$ and $f_k(2\pi)$ vanish. The following system was selected

$$f_k(\theta) = \sin k\nu \qquad k = 1,2,3,\ldots,n \tag{31}$$

Here, by definition,

$$\nu = \pi(\theta - \theta_2)/(2\pi - \theta_2) \tag{32}$$

It is noted that $0 \leq \nu \leq \pi$ for $\theta_2 \leq \theta \leq 2\pi$.

The coefficients C_k determined in this manner are next substituted into Eq. (26) to yield the modified w_a distri-

bution in the correction interval. Equation (13) is then used in reverse in this interval to determine s with θ known. Thus an acceptable modified $w_a(s)$ is obtained. This w_a automatically satisfies the circulation integral.

C. Airfoil Shape

To calculate the airfoil ordinates, the inclination angles of the velocity vectors along the surface must first be determined. With w_a known along the circle, τ may be calculated[2] from Poisson's integral, i.e.,

$$\tau(\theta) = \alpha + \frac{1}{2\pi}\int_0^{2\pi} \ln w_a \, ctn\frac{\theta - \theta'}{2} d\theta' \qquad (33)$$

Here the principal value of the integral must be taken at $\theta = \theta'$. It is noted that there exists a discontinuity in τ equal to π at the leading-edge stagnation point, i.e., at $\theta = \pi + 2\alpha$. There is also a discontinuity in τ from $\theta = 2\pi$ to 0, when the trailing edge of the airfoil is required to have a finite angle, i.e., when w_a at the trailing edge equals zero. If the velocity at the trailing edge is non-zero, the angle τ at $\theta = 2\pi$ equals that at $\theta = 0$. The airfoil then exhibits a cusp at the trailing edge.

The shape of the airfoil is obtained from the following integrals

$$x = \mp\int_0^s \cos\tau ds \qquad (34)$$

$$y = \mp\int_0^s \sin\tau ds \qquad (35)$$

The plus and minus signs apply to $0 \le \theta \le \pi + 2\alpha$ and $\pi + 2\alpha \le \theta \le 2\pi$, respectively. The resulting airfoil appears in the zero-lift position as far as our axis system is concerned. A simple rotation of the axes yields the surface ordinates measured from the chord, defined in the usual manner as the longest distance between a point on the leading edge and the trailing edge point.

D. Off-Design Velocity Distribution, Lift, and Pitching Moment

Remembering that the velocity at infinity equals unity, the lift may be expressed as both $\rho\Gamma$ and $\rho C_L c/2$ where C_L and c denote the lift coefficient and the chord, respectively. Hence, using Eq. (5)

$$C_L = 2\Gamma/c = 8\pi(R/c)\sin\alpha \qquad (36)$$

In the above development the angle-of-attack α is measured from the x-axis. The x-axis coincides with the zero-lift direction of the airfoil. Conventionally the angle-of-attack is measured from the airfoil chordline. The incremental $\Delta\alpha$ (always negative) between the x-axis and the chordline therefore corresponds to the usual angle of zero lift. In the numerical results presented in the next section the angles of attack shown, termed α_c, are equal to $\alpha + \Delta\alpha$ to conform to conventional practice.

The off-design velocity distribution is easily obtained by noting that Eqs. (7) and (8) may be rewritten as follows:

$$w_c = \pm 4\cos\left(\frac{\theta}{2} - \alpha\right)\sin\frac{\theta}{2} \qquad (37)$$

Substitution of Eq. (37) into Eq. (3) yields

$$w_a = \pm 4\cos\left(\frac{\theta}{2} - \alpha\right)\cdot\sin\left(\frac{\theta}{2}\right)\cdot\frac{Rd\theta}{ds} \qquad (38)$$

Upper surface		Lower surface	
x/c	y/c	x/c	y/c
0	0	0	0
.0044	.0033	.0048	-.0152
.0114	.0232	.0106	-.0206
.0198	.0320	.0240	-.0237
.0488	.0541	.0459	-.0273
.1030	.0815	.1069	-.0366
.1607	.1005	.1652	-.0399
.2005	.1093	.2090	-.0397
.2607	.1167	.2632	-.0377
.3214	.1160	.3193	-.0344
.3805	.1019	.3972	-.0281
.4100	.0943	.4171	-.0263
.4395	.0868	.4374	-.0243
.5186	.0690	.5200	-.0164
.5981	.0524	.6044	-.0089
.6978	.0341	.6914	-.0027
.7901	.0203	.7800	.0023
.8949	.0082	.8917	.0042
.9540	.0031	.9579	.0026
1.0000	0	1.0000	0

L.E. radius = 1.9 percent c

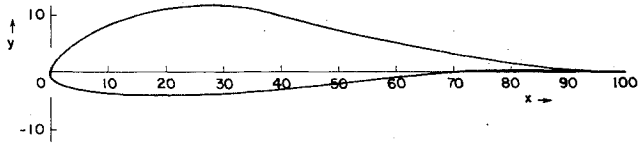

Fig. 3. Airfoil shape corresponding to velocity distribution of Fig. 2, $Re = 3.10^6$, $\Gamma = 68$. $C_L = 1.38$ $\alpha_c = 8.7°$, $C_{m0} = -0.05$, $t/c = 0.155$, $r/c \simeq 0.9\,(t/c)^2$, $L/D \simeq 96$ (turbulent flow).

We shall now retain the same mapping function, i.e., R, θ, and s remain unchanged, and change the angle of attack. The velocity distribution w_a at an arbitrary angle α is, therefore, given in terms of the design distribution w_{ad} and design angle of attack α_d by the following relation.

$$w_a = w_{ad}\left|\frac{\cos[(\theta/2) - \alpha]}{\cos[(\theta/2) - \alpha_d]}\right| \qquad (39)$$

This expression was given previously for $\alpha_d = 0$ in Ref. 2. The velocity distribution of the airfoil at any off-design angle-of-attack is now immediately known as a function of s. Specifically, the velocity distribution at zero lift is obtained by setting $\alpha = 0$

$$w_a\Big|_{C_L=0} = w_{ad}\left|\frac{\cos\theta/2}{\cos[(\theta/2) - \alpha_d]}\right| \qquad (40)$$

With this information the general expression for zero-lift pitching moment coefficient, derived in Ref. 2, may be used.

$$C_{m0} = -\frac{4R^2}{c^2}\int_0^{2\pi} \ln w_a\Big|_{C_L=0} \sin 2\theta d\theta \qquad (41)$$

III. Calculations

The expressions presented in the previous section were programmed on a CDC 3600 high-speed digital computer at the University of California, San Diego. A sample upper and lower surface input is shown in Fig. 2. It is convenient to attempt to have the chord length of the airfoil become approximately 100. This will in most cases correspond to a total upper surface length of around 106 and a lower surface length of around 100. Then the lift coefficient $C_L \simeq \Gamma/50$ by Eq. (36). It is also convenient, as pointed out in Ref. 3, to be able to change Γ without changing the input velocity distribution. In this case a contraction or expansion of the distance intervals between points 2 and 3 on the lower surface must be performed by the computer, so as to have

$$\Delta s_j \to \frac{G_{02} - \Gamma}{G_{23}}\Delta s_j \qquad (45)$$

where, by definition

$$G_{02} = \int_0^{s_2} w_a ds$$
$$G_{23} = \int_{s_2}^{s_3} w_a ds \qquad (46)$$

The $n + 5$ linear algebraic equations [Eq. (30)] may easily be shown to reduce the following matrix equation to

be solved for $C_1, \ldots, C_n$ and $\lambda_1, \ldots, \lambda_5$. Note that the matrix is symmetric.

$$\begin{bmatrix} \pi & 0 & 0 & 0 & 0 & & \frac{2}{1} & \frac{1(\cos\theta_2+1)}{1-A^2} & \frac{1\sin\theta_2}{1-A^2} & 1 & -1 \\ 0 & \pi & 0 & 0 & 0 & & 0 & \frac{2(\cos\theta_2-1)}{4-A^2} & \frac{2\sin\theta_2}{4-A^2} & 2 & 2 \\ 0 & 0 & \pi & 0 & 0 & & \frac{2}{3} & \frac{3(\cos\theta_2+1)}{9-A^2} & \frac{3\sin\theta_2}{9-A^2} & 3 & -3 \\ 0 & 0 & 0 & \pi & 0 & \text{etc.} & 0 & \frac{4(\cos\theta_2-1)}{16-A^2} & \frac{4\sin\theta_2}{16-A^2} & 4 & 4 \\ 0 & 0 & 0 & 0 & \pi & & \frac{2}{5} & \frac{5(\cos\theta_2+1)}{25-A^2} & \frac{5\sin\theta_2}{25-A^2} & 5 & -5 \\ & & \text{etc.} & & & & & & & & \\ \frac{2}{1} & 0 & \frac{2}{3} & 0 & \frac{2}{5} & & & \text{etc.} & & & \\ \frac{1(\cos\theta_2+1)}{1-A^2} & & \text{etc.} & & & & & & & & \\ \text{etc.} & & & & & & & & & & \end{bmatrix}$$

$$\times \begin{bmatrix} C_1 \\ C_2 \\ C_3 \\ C_4 \\ \text{etc.} \\ \lambda_1 \\ \lambda_2 \\ \lambda_3 \\ \lambda_4 \\ \lambda_5 \end{bmatrix} = \begin{bmatrix} 0 \\ 0 \\ 0 \\ 0 \\ \text{etc.} \\ -\frac{1}{A}\int_0^{2\pi} \ln w_{a0} d\theta \\ -\frac{2\pi\sin^2\alpha}{A} - \frac{1}{A}\int_0^{2\pi} \ln w_{a0}\cos\theta d\theta \\ \frac{\pi\sin 2\alpha}{A} - \frac{1}{A}\int_0^{2\pi} \ln w_{a0}\sin\theta d\theta \\ 0 \\ 0 \end{bmatrix} \quad (47)$$

Here $A = 2 - \theta_2/\pi$, by definition.

Some care must be taken in the evaluation of the integrals on the right hand side of the above equation. From the evaluation of τ (described below), it was determined that the magnitude of the input slopes dw_{a0}/ds at the stagnation point must be equal on the upper and lower surfaces, otherwise the integral for τ is not convergent. Thus in the immediate neighborhood of the stagnation point we may write, for, respectively, the upper and lower surface

$$w_{a0} = \mp (dw_{a0}/ds \mid_{s=s_1})(s - s_1) \quad (48)$$

Integration of Eq. (3) yields (with the positive angle μ in the circle plane measured from the stagnation point)

$$w_{a0}(\theta) = k_1\mu[1 \pm k_2\mu - 0(\mu^2)]$$
$$\text{for} \quad \pi + 2\alpha - \epsilon \leq \theta \leq \pi + 2\alpha + \epsilon \quad (49)$$

where, by definition

$$k_1 = \left(2R \left.\frac{dw_{a0}}{ds}\right|_{s=s_1} \cos\alpha\right)^{1/2}$$
$$k_2 = (1/6)\tan\alpha \quad (50)$$

Substitution of the above expressions for w_{a0} into the integrands on the right hand side of the matrix equation yields, with $\epsilon \ll 1$

$$\int_{\pi+2\alpha-\epsilon}^{\pi+2\alpha+\epsilon} \ln w_{a0} d\theta = 2\epsilon \ln(k_1\epsilon) - 4\epsilon + \frac{1+k_2\epsilon}{k_2}\ln(1+k_2\epsilon) - \frac{1-k_2\epsilon}{2k_2}\ln(1-k_2\epsilon) \quad (51)$$

$$\int_{\pi+2\alpha-\epsilon}^{\pi+2\alpha+\epsilon} \ln w_{ao} \cos\theta d\theta = -\cos 2\alpha \left\{2\epsilon \ln(k_1\epsilon) - 4\epsilon + \frac{1+k_2\epsilon}{k_2}\ln(1+k_2\epsilon) - \frac{1-k_2\epsilon}{k_2}\ln(1-k_2\epsilon)\right\} + \sin 2\alpha \left\{\frac{k_2^2\epsilon^2-1}{2k_2^2}\ln(1-k_2\epsilon) - \frac{\epsilon}{k_2} - \frac{k_2^2\epsilon-1}{2k_2^2}\ln(1+k_2\epsilon)\right\} \quad (52)$$

$$\int_{\pi+2\alpha-\epsilon}^{\pi+2\alpha+\epsilon} \ln w_{ao} \sin\theta d\theta = -\sin 2\alpha \left\{2\epsilon \ln(k_1\epsilon) - 4\epsilon + \frac{1+k_2\epsilon}{k_2}\ln(1+k_2\epsilon) - \frac{1-k_2\epsilon}{k_2}\ln(1-k_2\epsilon)\right\} + \cos 2\alpha \left\{\frac{k_2^2\epsilon^2-1}{2k_2^2}\ln(1+k_2\epsilon) + \frac{\epsilon}{k_2} - \frac{k_2^2-1}{2k_2^2}\ln(1-k_2\epsilon)\right\} \quad (53)$$

After solving the matrix equation, the modified set of w_a's [Eq. (26)] is next employed to calculate a new set of s for $s_2 < s < s_3$, using Eq. (13), while maintaining unaltered the set of θ. No iterations are needed.

Special expansions are also required to evaluate the τ-integral. Here it is first convenient to express τ in an equivalent form, namely

$$\tau = \alpha + \int_0^{2\pi} \ln\left[\frac{w_a(\theta')}{w_a(\theta)}\right] ctn\frac{\theta-\theta'}{2} d\theta' \quad (54)$$

A straight line is then drawn between neighboring points of the set of w_a and also of the set of $ctn[(\theta - \theta')/2]$. Thus, the integral is reduced to the type

$$\sum \int_0^{\Delta\theta} \ln[a(\theta) + b(\theta)\cdot x][A(\theta) + B(\theta)\cdot x]dx]$$

Closed form expressions of this integral are readily obtainable.

In Fig. 2 a trailing edge velocity of 0.95 and a stagnation point slope $dw_a/ds = 0.6$ have been used. A Stratford[4] zero-skinfriction distribution for $Re = 3.10^6$ was calculated for the aft portion of the upper surface. Turbulent flow was assumed for the whole airfoil. The s_2-distance was chosen to be 106.3 ($s_1 = 106$). The dashed line on Fig. 2 indicates the input velocity distribution along the lower surface. The acceptable (modified) velocity distribution along the lower surface, as calculated by the computer, is given by the heavy line. It was found that the irregularities (small waviness) in the curve could be minimized by using a large number of terms in the series expansion. The curve shown was obtained with a 35 × 35 matrix equation ($n = 30$). The wave amplitudes were approximately double of those shown when using $n = 20$, instead of $n = 30$.

The corresponding airfoil is presented in Fig. 3. It has the characteristic humpback look of the Liebeck-Ormsbee airfoils.[1] The lower surface is slightly convex in front with a reflexed portion near the trailing edge. The lift coeffi-

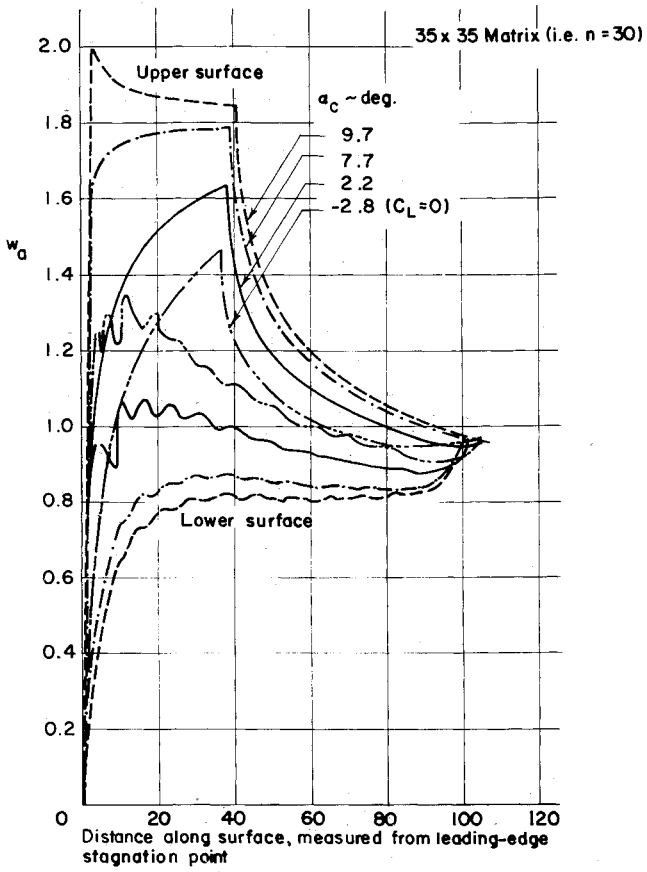

Fig. 4. Off-design velocity distributions for the airfoil of Fig. 3.

cient is 1.38 with $\alpha_c = 8.7°$ and a maximum thickness ratio of 0.155. The zero-lift pitching moment coefficient is a satisfactorily low −0.05. The predicted turbulent-flow

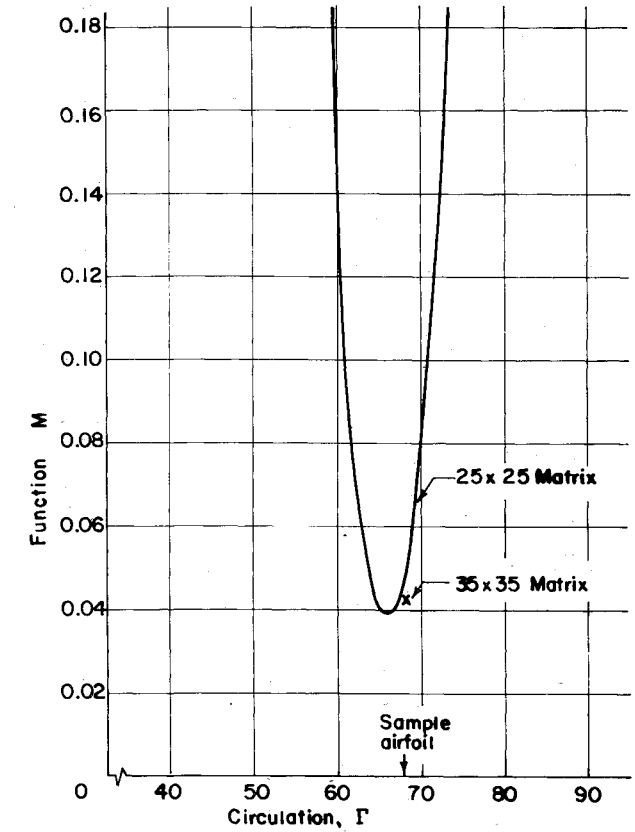

Fig. 5. Effect of varying Γ on minimizing M-function.

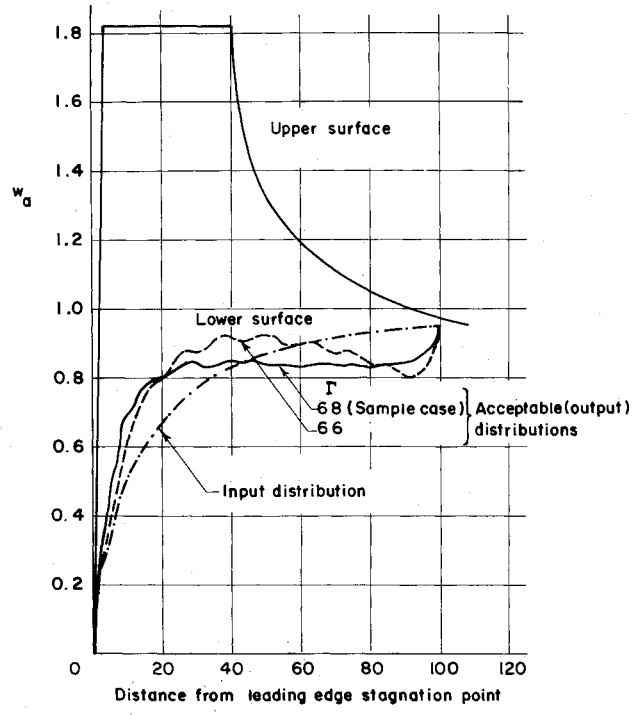

Fig. 6. Effect of varying input Γ on lower-surface velocity distribution.

lift/drag ratio is 96, which is at least 50% higher than that obtained by tests on conventional airfoils at corresponding lift coefficients. Since the shape of the lower surface is mostly convex, the angle-of-attack range for attached flow should be satisfactory for the sample airfoil.

Off-design velocity distributions are presented in Fig. 4. The highest angle shown ($\alpha_c = 9.7°$) is one degree more than the design angle of attack. The profile should therefore exhibit separated flow over the entire aft portion of its upper surface, rather than the distribution shown, due to boundary layer effects. The design angle of attack does not, however, necessarily correspond to the maximum lift coefficient of the profile. Additional lift at angles of attack beyond the design lift coefficient might be expected because of the so-called "elastic" property of the boundary layer displacement thickness, found experimentally by Stratford. The design lift coefficient must therefore be considered as being the limit (maximum) coefficient in the essentially linear range of C_L vs α. The velocity distribution for the lowest angle shown on Fig. 4 indicates a negative C_{m0}, which is in accordance with that calculated by the Lighthill integral. The off-design velocity distributions appear to be both reasonable and satisfactory for a turbulent flow airfoil. The maximum velocity (of the order of 1.5) on the upper surface for low positive lift coefficients is higher than the maximum velocities of the NACA high-speed sections, but not much different from those of the earlier NACA four- and five-digit series, still used in many aircraft and helicopter applications. Presumably, the advantage of the sample profile over the NACA four- and five-digit airfoils of corresponding thickness ratio would lie in its predicted low drag up to the

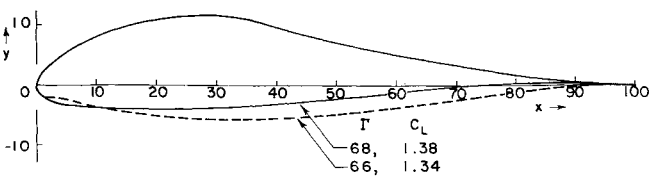

Fig. 7. Effect of varying Γ on airfoil shape.

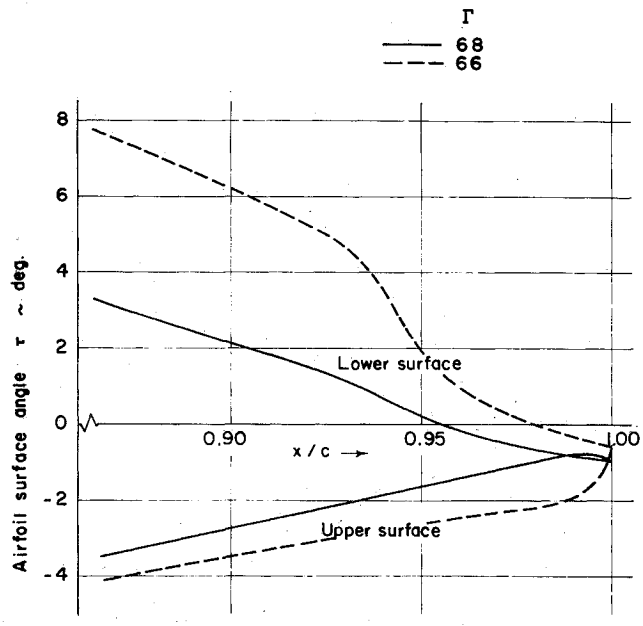

Fig. 8. Effect of varying Γ on airfoil surface angles near the trailing edge.

highest lift coefficient in the linear range (C_L = 1.38 at the design Reynolds number of 3.10^6). This should be a direct result of taking the major portion of the upper-surface velocity decrease at a far forward location where the boundary layer is still relatively thin. The low drag would be obtained from the zero-skinfriction feature along the upper aft portion of the airfoil. The decrease in friction drag would possibly be partially offset by a slight increase in form drag due to an increase in the boundary layer thickness. Note that there exists a favorable pressure gradient, conducive to laminar flow, along the upper surface ahead of the Stratford distribution at all angles of attack up to the design angle.

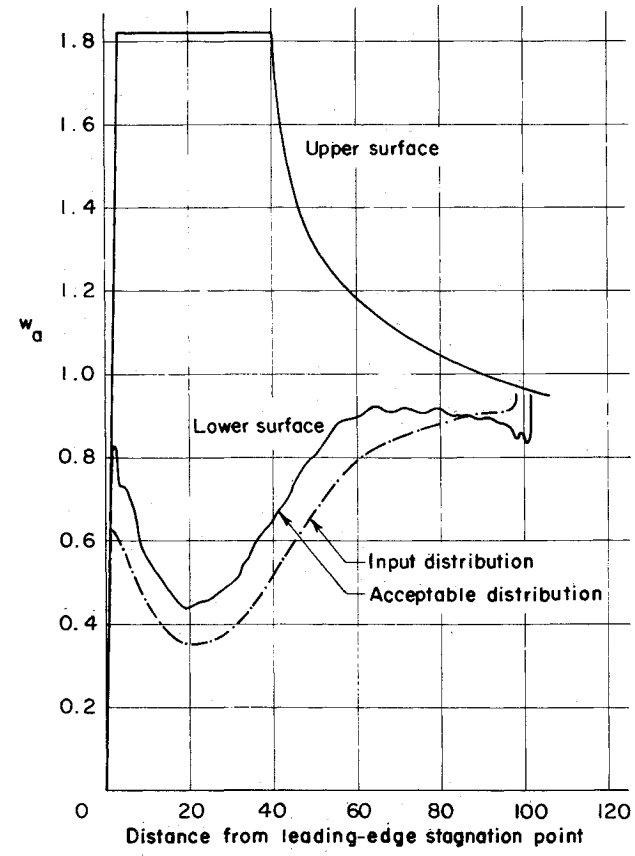

Fig. 9. A different lower-surface velocity distribution, Re = 3.10^6, Γ = 71 for the acceptable distribution.

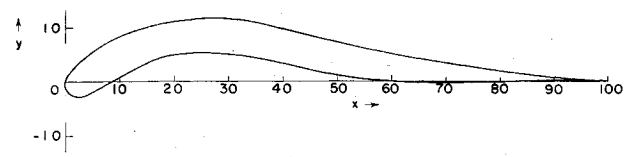

Fig. 10. Airfoil shape obtained from velocity distribution of Fig. 9. Re = 3.10^6, Γ = 71, C_L = 1.44, α_c = 8.9°, C_{m0} = −0.037, t/c = 0.07, $r/c \simeq 4\,(t/c)^2$, $L/D \simeq$ 100 (turbulent flow).

In every calculation attempted, it was found necessary to first perform a survey with Γ as the variable. The result of the survey, leading to the choice of the sample profile, is presented in Fig. 5, where the minimizing function M is plotted vs Γ. When M is small, the modified velocity distribution will be close to the given input distribution on the lower surface. Also indicated in the figure is the rather small decrease in M due to the use of an increased number of terms in the series expansion for the velocity.

The effects of reducing Γ from 68 to 66, using the same input as before, are given in Figs. 6 and 7. The sensitivity of the shape of the lower-surface of the profile to relatively small changes in the lower-surface velocity distribution is noted. It was also found that the upper surface shape is essentially unchanged by any alterations in the acceptable distributions on the lower surface. This may be explained by the fact that the angle of attack, as determined from Eq. (11), is not greatly affected by minor changes in Γ.

The slopes of the airfoil surface near the trailing edge should probably, for a good airfoil, show a somewhat regular variation with aft distance, since the inviscid flow effect of rapid changes in slopes there might easily be hidden inside the relatively thick boundary layer. Figure 8 indicates that for the sample airfoil (Γ = 68) the slopes are a linear function of distance. However, a small change in Γ from 68 to 66, destroys the linearity as indicated in the figure.

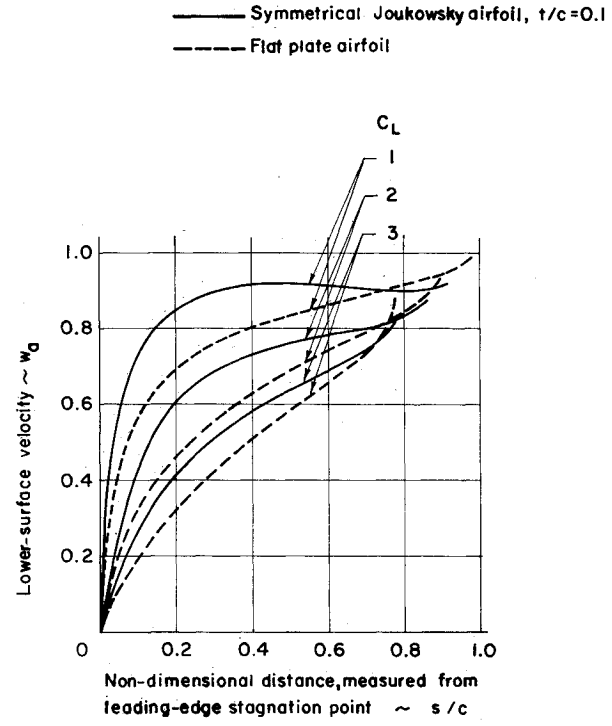

Fig. 11. Velocity distribution on the lower surface of a flat plate and of a symmetrical Joukowsky airfoil of 10% maximum thickness ratio.

Next, a lower-surface distribution (Fig. 9), identical to that used to design the airfoil tested by Pick and Lien,[5] was used as input to obtain a thin airfoil (Fig. 10), having the same upper-surface Stratford distribution as that shown in Fig. 2. As expected, there were essentially no changes in the upper-surface contour. The lower surface exhibits a large amount of concavity. The large slopes of the surface inside this cavity are not, of course, conducive to attached flow at the lower angles of attack. Thus, as found experimentally by Pick and Lien, separated flow exists in this region at angles of attack lower than 4–5° leaving a range of only about 5° of good flow. This is, however, a feature of all highly cambered thin airfoils in use. Encouraging results were reported by Pick and Lien in their experimental investigation of the validity of the Stratford incipient-separation criterion as applied to the design of airfoils.

Additional test data of a very encouraging nature have been obtained by Bingham and Chen[6] and Liebeck.[7]†

Figure 11 has been included as an aid in selecting the input lower-surface velocity distribution. To obtain an almost flat lower surface, it is probable that an input distribution close to that of a flat plate at the same angle of attack would have to be used. Similarly, to obtain a slightly convex lower-surface contour, an input distribution close to that of a Joukowsky symmetrical airfoil would have to be used.

IV. Conclusions

The Lighthill-Arlinger method has been extended by the use of a least squares technique combined with Lagrangian multipliers to obtain a lower surface velocity distribution that will consistently produce acceptable airfoil shapes. The method is exact in the sense of potential flow theory, and may therefore be used to advantage to calculate the shapes of new airfoils with high design lift coefficients, i.e., under conditions when conventional first- and second-order linearized theory breaks down. Thus a valuable tool for future design of specialized wing sections has been developed.

The new method has been employed in a sample calculation to find the shape of several high-lift low-drag airfoils, having lift/drag ratios of around 100 in all-turbulent flow at design lift coefficients of around 1.4. In the sample calculation the stress was on showing that airfoils of reasonable shape could be determined through the new method. No effort was made to maximize the design lift coefficient or the lift/drag ratio. Much larger design lift coefficients and L/D's are available.

† This paragraph and these references were added to the text after the paper had been returned to the author for minor revisions.

References

[1]Liebeck, R. H. and Ormsbee, A. I., "Optimization of Airfoils for Maximum Lift," *Journal of Aircraft*, Vol. 7, No. 5, Sept.–Oct. 1970, pp. 409–415.

[2]Lighthill, M. J., "A New Method of Two-Dimensional Aerodynamic Design," R&M 2112, April 1945, Aeronautical Research Council, London, England.

[3]Arlinger, G., "An Exact Method of Two-Dimensional Airfoil Design," TN 67, Oct., 1970, Saab, Linköping, Sweden.

[4]Stratford, B. S., "The Prediction of Separation of the Turbulent Boundary Layer," *Journal of Fluid Mechanics*, Vol. 5, 1959, pp. 1–16.

[5]Pick, G. S. and Lien, D. A., "The Development of a Two-Dimensional High-Endurance Airfoil with Given Thickness Distribution and Reynolds Number," Sept. 1972, Naval Ship Research and Development Center, Aviation and Surface Effects Dept., Washington, D.C.

[6]Bingham, G. J. and Chen, A. W., "Low-Speed Aerodynamic Characteristics of an Airfoil Optimized for Maximum Lift Coefficient," TN D-7071, Dec. 1972, NASA.

[7]Liebeck, R. H., "A Class of Airfoils Designed for High Lift in Incompressible Flow," AIAA Paper 73-86, Jan. 1973, Washington, D.C.